Vis-NIR electrochromism and NIR-green electroluminochromism in dual functional benzothiadiazole-arylamine mixed-valence compounds

*Giuseppina Anna Corrente, Dora A. González, Ece Aktas, Agostina Lina Capodilupo, Gloria Mazzone, Francesco Ruighi, Gianluca Accorsi, Daniela Imbardelli, Cristina Rodriguez-Seco, Eugenia Martinez-Ferrero, Emilio Palomares, and Amerigo Beneduci**

Dr. G. A. Corrente, Dr. G. Mazzone, Dr. D. Imbardelli, Prof. A. Beneduci
Department of Chemistry and Chemical Technologies, University of Calabria, Via P. Bucci, Cubo 15D, 87036 Arcavacata di Rende, Italy
E-mail: amerigo.beneduci@unical.it

D. A. González, Dr. E. Aktas, Dr. C. Rodriguez-Seco, Dr. E. Martinez-Ferrero, Prof. E. Palomares
Institute of Chemical Research of Catalonia, The Barcelona Institute of Science and Technology (ICIQ-BIST), E-43007 Tarragona, Spain;
Departament d'Enginyeria Electrònica, Elèctrica i Automàtica. Universitat Rovira i Virgili, Avda. Països Catalans, 26, Tarragona, E-43007, Spain

Dr. E. Aktas
Current address: Department of Chemical, Materials and Production Engineering, University of Naples Federico II, Piazzale Tecchio 80, 80125 Fuorigrotta, Italy

Dr. C. Rodriguez-Seco
Current address: Énergie Matériaux et Télécommunications, Institut National de la Recherche Scientifque (INRS), Varennes, QC, Canada.

Dr. A. L. Capodilupo, Dr. F. Ruighi, Dr. G. Accorsi
Institute of Nanotechnology (CNR-NANOTEC), c/o Campus Ecotekne, via Monteroni, 73100 Lecce, Italy

Prof. E. Palomares
Catalan Institution for Research and Advanced Studies (ICREA), 08010 Barcelona, Spain

Keywords: (benzothiadiazole, mixed-valence compounds, Vis-NIR absorption, photoluminescence, electrochromism, electrofluorochromism)

Abstract
Electrochromism/Electrofluorochromism is the reversible tuning of the absorption/photoluminescence by redox processes. Dual functional electrochromic/electrofluorochromic materials can be exploited in e.g., smart windows, encryption/anticounterfeiting technologies, displays and biomedical sensors. While electrofluorochromic materials showing tunable fluorescence intensity, are relatively widespread, those with tunable color emission are not. Moreover, electrofluorochromic materials with tunable emission in the near-infrared range, are seldom encountered. Here we show a new molecular approach to afford both the above functionalities, in addition to red-NIR electrochromism, by combining the properties of highly stable arylamine radical cation mixed valence species, with those of donor-acceptor systems exhibiting the photoinduced twisted intramolecular charge transfer (TICT) mechanism.

1. Introduction

Electrochromism (EC) and electrofluorochromism (EFC), which refer to the reversible switching of absorption and fluorescence signals in response to an electric stimulus,[1-4] have gained great interest for potential applications in tinting eyeglasses and windows in buildings, cars, or airplanes,[5-8] memory displays,[9-12] wearable electronics, energy storage,[13-14] information encryption, bioanalysis, and sensors.[15-17] To date, there is a significant focus on organic conjugated materials because of their high contrast, fast response, processability, and cost-efficiency.[18-20] In this context, an open issue is the stability of the electroactive molecules subject to several electrochemical redox cycles. Recently, compounds containing two or more arylamine redox centres connected through a π-conjugated bridge are being investigated due to their excellent reversible redox switching cyclability from the neutral state to the oxidised radical-cation mixed-valence (MV) state, which is characterized by a high stability thanks to the electronic coupling between the redox centers.[21,22] In these systems, the π-conjugated bridging unit plays a crucial role in exploiting the electrochromic response in the near-infrared region (NIR), by optically-inducing the Intervalence Charge Transfer Transition (IVCT).[22]

Another challenge is to develop dual functional electrochromic/electrofluorochromic materials where the bridging unit should be a suitable fluorophore.[23,24] It is worth noting that most of the electrofluorochromic materials reported so far, undergo a mere photoluminescence quenching mechanism. Therefore, another intriguing issue is to achieve a voltage-dependent tuning of the emission wavelength, also known an electroluminochromic effect.[25-29] Herein, we propose a new approach to cope with the above challenges using the benzothiadiazole (BT) group as fluorophore bridging unit in materials with a Donor-Acceptor-Donor (DAD) structure where the donor units are both arylamines derivatives. Recently, a push-pull benzothiadiazole fluorophore, consisting of a benzothiadiazole core, a terminal N,N-dimethylamino electron donating group and a terminal electron withdrawing group (–NO_2 and –CN), has been reported to show electrochromic and electrofluorochromic properties, with interesting electrochemical tuning of the fluorescent intensity and wavelength.[30] However, to the best of our knowledge, bis-arylamine mixed valence compounds with the benzothiadiazole bridge, have never been studied as electrofluorochromic and electrochromic material, while they have already been extensively investigated in the field of photovoltaics[31-43] and LED.[44-49] Therefore, due to the high fluorescence properties of the benzothiadiazole, its strong electron-withdrawing nature and its easy functionalization with arylamine units,[31-32-50] the benzothiadiazole fluorophore may be usefully explored in arylamine mixed valence compounds, by taking advantage of the occurrence of intramolecular charge transfer processes between the arylamine units and the electron deficient bridge.[51-52] This would allow an improvement of their EC and EFC response by tuning the intramolecular and intervalence charge transfer processes upon oxidation, and to shift the light emission toward the red-NIR range, thus affording electrofluorochromic systems that may be explored in the biomedical field.[53, 54]

Figure 1 reports the structures of the BT based small molecules, where the electron-acceptor BT core is covalently linked to two electron-donor diphenylamine (DPA) or triphenylamine units (TPA), designing donor-acceptor-donor compounds of the type BTDPA (molecules CS01 and CS03) and BTTPA (molecules EP02 and LCS01).[32] The rationale design of these compounds is therefore based on the choice of different bridging unit (benzothiadiazole, phenyl-benzothiadiazole-phenyl) connecting the arylamine redox centres, and of the substituents on the phenyl groups of the arylamines (methoxy, phenyl, dimethoxyphenyl). In this way, the effects of varying the length of the bridge (benzothiadiazole *vs.* phenyl-benzothiadiazole-phenyl) connecting the N-atoms, and of varying the nature of the substituents on the arylamine (methoxy, phenyl, dimethoxyphenyl), on the electrochromic and electrofluorochromic properties, can be investigated.

Here we show that these systems combine the properties of arylamine MVs, characterized by high stability of the radical cation species, with the properties of donor-acceptor systems exhibiting the

photoinduced TICT mechanism. The results are dual functional materials with red-NIR electrochromism and red-NIR electroluminochromism with a huge electrofluorochromic quenching efficiency and a voltage-dependent colour tuning of the fluorescence emission from red to green.

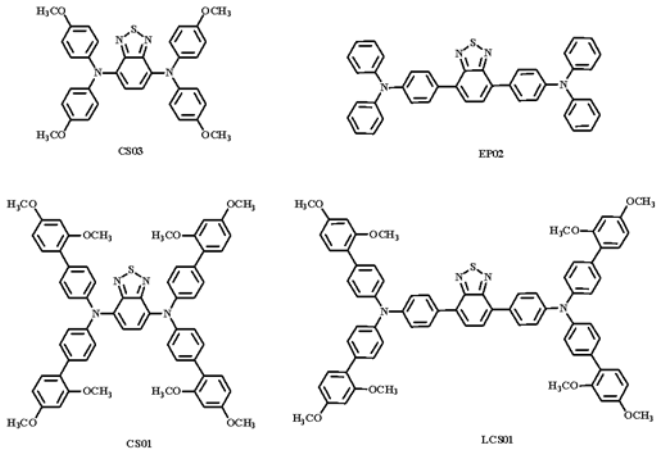

Figure 1. Chemical structures of benzothiadiazole based arylamine mixed valence derivatives.

2. Results and discussion

2.1. Photophysical investigation

The steady state and time resolved photophysical properties of the DAD compounds were investigated in different solvents. The absorption spectra show a large UV absorption (< 350 nm; $10000 < \varepsilon < 60000$ M^{-1} cm^{-1}) attributed to a π–π^* transition and a broad and relatively intense ($6000 < \varepsilon < 40000$ M^{-1} cm^{-1}), lower energy transition centred at about 450 nm and 550 nm, for the BTDPA and BTTPA systems, respectively (**Figure 2**, **Table 1** and **Figure S1**). The latter arising from an intramolecular charge transfer from the arylamine (D) to the BT core (A).[55-56] The position of this transition depends on the donor unit and it is shifted to longer wavelengths in the bisarylamine triads, where the electron donating effect is stronger. This highlights that it can be potentially tuned by changing the substituents on the phenyl rings and/or by introducing different π-conjugated spacers between the BT bridge and the arylamine moieties. Time-dependent density functional theory (TDDFT) calculations confirm the assignment of the low-energy absorption region, arising from the HOMO-LUMO transition, as an intramolecular charge transfer excitation from the donor arylamine to the acceptor BT core and that the most intense band in the UV region is centred on the π system for all the compounds (**Table S1** and **Figure S2**). The absorption data show that the CT ground state of the compounds CS03 and CS01 is quite insensitive to the increase of the solvent polarity, with a blue shift of 5 nm and 9 nm, respectively. This solvatochromism is slightly enhanced in LCS01 and EP02 with blue shifts of 23 nm and 21 nm, respectively.

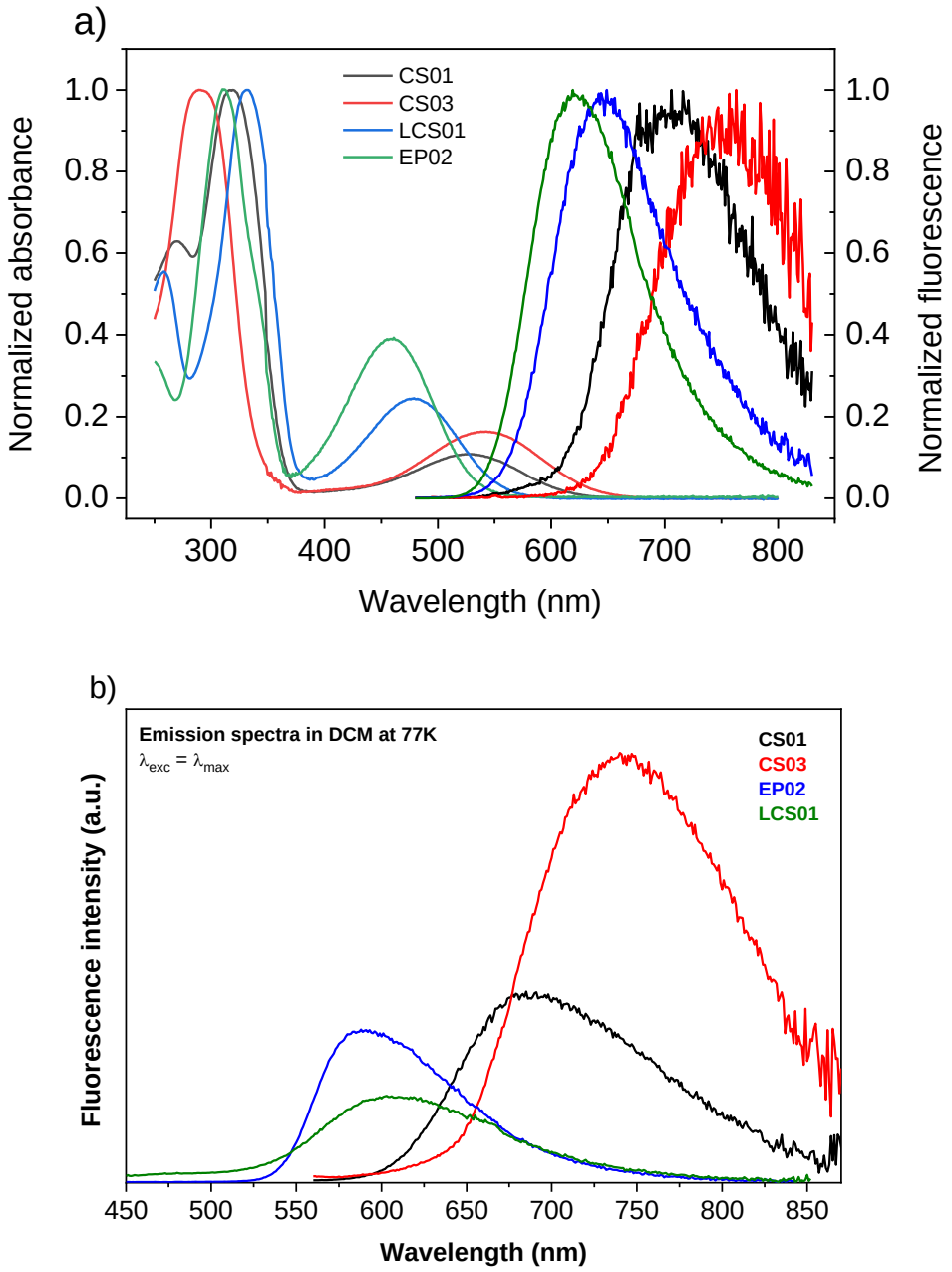

Figure 2. a) Absorption and corrected emission spectra of CS01 (λ_{ex} = 528 nm), CS03 (λ_{ex} = 540 nm), LCS01 (λ_{ex} = 460 nm), and EP02 (λ_{ex} = 450 nm) molecules in tetrahydrofuran. b) Emission spectra of CS01, CS03, LCS01, and EP02 in dichloromethane at 77K rigid matrix ($\lambda_{ex} = \lambda_{max}$).

Analogously to the absorption, the fluorescence spectra exhibit considerable charge-transfer character, leading to broad emission bands, shifted far in the red-NIR region (Figure 2). This is also corroborated by the absence of vibronic structures even in the most apolar solvent of the series, and by the very large Stokes shifts of the excited states (3600-7900 cm^{-1}) (Table 1), that is comparable to those observed in

twisted intramolecular charge transfer (TICT) donor-acceptor fluorophores[55-57] and in dibenzo[*a*,*c*]phenazin-11-yl(phenyl)methanone (PM) based arylamine MVs.[31,58]

Deconvolution of the fluorescence spectra reveals that there is a superposition of two bands in the vis range and a third in the NIR region, which are monotonically shifted toward NIR with the solvent polarity (**Figure S3** and **Table S2**). These spectral features may arise from the presence of at least three different emitting species in equilibrium, that is rapidly established after excitation. The different emitting species reflect the generation of charge transfer states of different energy, that could be determined by the intramolecular twisting of the arylamine units relative to the benzothiadiazole bridge (TICT), as already observed in similar systems where different conformers were established for the excited state.[59,60]

To this purpose, we acquired the emission profiles (**Figure 2b**) and the corresponding lifetime decays (Table 1) in dichloromethane at 77 K for all the compounds in order to prove the presence of different species by blocking the rotations of the arylamine units. In fact, we found biexponential decays when acquired at shorter wavelengths (Table 1) changing to monoexponential at lower energy. This is in agreement with the deconvoluted emission spectra (77 K, **Figure S4**) where two emission bands are present in the higher energy spectral region. On the contrary, at longer wavelengths, only one remains leading to the presence of an equilibrium between rotomers in the molecular structures.

On the other hand, a monoexponential function can satisfactorily fit the fluorescence decay behaviour at room temperature (Table 1), since the calculated energy barrier to rotation of the aryl amine unit relatively to the benzothiadiazole, are sufficiently low (less than 23 kJ/mol) to allow for a rapid interconversion among the different conformers within the excited state lifetime, as already observed on similar DAD benzothiadiazole systems.[61]

Table 1. Fluorescence quantum yields (FLQY), fluorescence lifetimes (τ_{obs}) and values of radiative and non-radiative decay constants (k_r and k_{nr}) of BTDPA and BTTPA compounds in different solvents.

CS03										
Solvent	λ_{max} $\pi-\pi^*$ (nm)	λ_{max} ICT (nm)	λ_{em} (nm)	Stokes Shift (cm^{-1})	FLQY (%)	τ_{obs} (ns)	k_r (10^{-11}) $s^{-1a)}$	k_{nr} (10^{-11}) $s^{-1a)}$	τ_{obs} (ns) 77 K λ_{em} = higher energy	τ_{obs} (ns) 77 K λ_{em} = lower energy
MCH	294	545	725	4556	7.0	7.3	0.96	12.7	/[d]	/
THF	291	543	757	5206	3.4	3.6	0.94	26.8	/	/
DCM	293	550	776	5295	0.4[c]	nd[b)]	nd	nd	λ_{em} = 650 nm 3.3 (9%) 13.6 (91%	λ_{em} = 800 nm 8.4
ACN	287	536	791	6015	0.2[c]	nd	nd	nd	/	/
CS01										
MCH	319	530	671	3965	18.0	11.3	1.60	7.26	/	/

THF	317	527	706	4811	15.0	9.3	1.61	9.14	/	/
DCM	317	532	756	5570	1.5[c]	3.9	0.38	25.3	λ_{em} = 650 nm 3.6 (8.5%) 15.2 (91.5%)	λ_{em} = 800 nm 13.0
ACN	316	520	774	6311	1.3[c]	4.3	0.30	23.0	/	/
LCS01										
MCH	334	485	587	3583	69.0	5.6	12.3	5.53	/	/
THF	332	477	649	5556	47.0	6.2	7.58	8.55	/	/
DCM	333	467	677	6642	5.7	2.5	2.28	37.7	λ_{em} = 530 nm 2.0 (42%) 6.7 (58%)	λ_{em} = 750 nm 6.7
ACN	326	462	729	7928	0.3	nd	nd	nd	/	/
EP02										
MCH	312	460	573	4287	66.0	6	11.0	5.67	/	/
THF	312	459	621	5683	63.0	7.3	8.63	5.07	/	/
DCM	312	460	649	6331	51.0	7.7	6.62	6.36	λ_{em} = 550 nm 1.6 (14%) 6.0 (86%)	λ_{em} = 700 nm 8.3
ACN	309	449	672	7391	26.0	4.9	5.31	15.1	/	/

[a)]Calculated by the equation $FLQY = k_r\tau_{obs}$ and $\tau_{obs} = \frac{1}{k_r+k_{nr}}$; where k_r and k_{nr} are the radiative and non-radiative decay constants; [b)]nd = not detected; [c)]Values underestimated because they do not include the emission in the NIR range. [d)]Not performed.

Moreover, the TICT mechanism is supported by a tiny increase of the energy of the ICT absorption band ($\Delta\lambda_{max}$ < 25 nm), in contrast to a large red shift of the emission band as a function of the solvent orientation polarizability (Table 1, **Table S3** and **Figure S5**). The data in Table 1 and the solvatochromism analysis by the Lippert-Mataga and the Bilot-Kawski models[59,60,62,63] (**Table S4** and **S5**, Figure S5 and **S6**) suggest that the dipole moment of the ground state (μ_g) is almost insensitive to the solvent polarity, while, that of the excited state (μ_e), is strongly dependent on it. There is, indeed, a significant increase of its value, leading to large dipole moment differences, ($\Delta\mu = \mu_e - \mu_g$) (**Table S6**), in agreement to other similar DAD compounds characterized by greater ICT character in the excited state.[55-57] Assuming the existence of conformers with different dipole moment in the excited state, the ones with the highest polarity are expected to be the most stabilized by the increase of the solvent polarity. Therefore, a monotonic decrease of the energy of the emission band (redshift as observed) is linked with a monotonic decrease of the radiative rate constant (k_r) and of the fluorescence quantum yield (FLQY), due to intramolecular rotation, which should be expected with the increase of the solvent polarity. Table 1 and Figure S5 show that this trend is well observed ongoing from methylcyclohexane (MCH) to acetonitrile (ACN), even though, the effect of the solvent is not the same across the compounds, with the EP02 showing the highest FLQY in all solvents. Notably, both CS01 and CS03 emit appreciably less than LCS01 and EP02. Computational calculations show that the most stable

conformation of the fluorophores in the ground state is tilted with dihedral torsion angles, defined according to the scheme in **Table S7**, of ~ 40° and ~ 50° respectively for the BTTPA and BTDPA fluorophores (Table S7). Interestingly, in the excited state, LCS01 and EP02 tend to become planar (~ 20°), while in CS03 and CS01 there is only a small tendency to planarization, and the tilted conformation is almost entirely kept. The higher fluorescence of the BTTPA fluorophores may be explained by their higher planarity which favours the charge transfer state. This is also reflected in the larger Stokes shifts observed for LCS01 and EP02, which are stabilized by higher solvent polarities. Accordingly, it is clear that the non-radiative deactivation pathways are more efficient in CS03 and CS01 compared to the other two systems, in all solvents. Thus, one of the most important quenching mechanisms may be due to intramolecular rotations, that seem to be more efficient in the BTDPA compounds where the arylamines are linked to the benzothiadiazole directly through the nitrogen atom, being the other conditions the same. Notably, the relative increase of the fluorescence of BTDPAs at 77 K, compared to that at room temperature, may be attributed to the restriction of intramolecular rotations corroborating, therefore, the hypothesis of the existence of rotomers at higher temperatures.

2.2. Electrochemistry

The electrochemical properties of these compounds were studied by cyclic voltammetry and differential pulse voltammetry in dichloromethane solution with $TBAPF_6$ as supporting electrolytes (**Figure S7** and **S8**). Cyclic voltammograms show reversible oxidations in the potential window between 0.4 and 1.5 V *vs.* AgCl/Ag (Figure S7). Specifically, the BTDPA compounds undergo two well separated one-electron oxidations (Figure S7 a and c). These two processes can be attributed to the sequential generation of the radical cation and radical dication species, respectively. The calculated potential splittings for these compounds are 358 and 302 mV, respectively (**Table 2**). In contrast, the expected two sequential oxidation processes cannot be clearly distinguished for the BTTPA systems, where they seem to be strongly overlapped (Figure S7 b and c). Indeed, differential pulse voltammetry analysis (DPV) revealed that the two processes are separated by less than 100 mV (Figure S8; Table 2). The deconvolution of the DPV curves confirms that both compounds undergo two one-electron oxidation processes, being the area of the two oxidation processes almost equivalent (Figure S8).

Table 2. Electrochemical Properties and Corresponding Energy Levels of the benzothiadiazole arylamines[a)]

Compound	$E_{1/2}(1)$ (mV)	$E_{1/2}(2)$ (mV)	ΔE_1[b)] (mV)	K_{CO} [c)]	E_{HOMO}[d)] (eV)	E_{LUMO}[e)] (eV)	E_g^{opg}(eV)
CS03	-35.5	322.7	358.2	1.2×10^6	-5.07	-3.17	1.90
CS01	139.2	441.3	302.1	1.3×10^5	-5.19	-3.2	1.99
LCS01	352[f)]	438[f)]	87	29	-5.23	-3.04	2.19
EP02	457[f)]	553[f)]	101	42	-5.44	-3.14	2.3

[a)] $c = 5 \times 10^{-4}$ mol/L in CH_2Cl_2/$TBAPF_6$ (0.1 M) *vs.* Fc^+/Fc at 100 mV/s for CS03 and EP02 and at 50 mV/s for CS01 and LCS01. [b)] $\Delta E = E_{1/2}(2) - E_{1/2}(1)$. [c)] $K_{CO} = e^{\Delta E/0.059}$. [d)] $E_{HOMO} = -(E_{onset(ox1)} + 5.16)$ (eV). [e)] $E_{LUMO} = E_g^{opt} - E_{HOMO}$. [f)] Peak maximum in the DPV (E_{pa}).

The large comproportionation constant K_{CO} (Table 2) of CS03 and CS01, evidences the good thermodynamic stability of the radical cation species relatively to the neutral and the dication ones, due to a strong electron coupling between the redox centers. The computed spin densities, indeed, evidenced the delocalization of the unpaired electron on the two N atoms and the carbon atoms lying among them as well as the carbon atoms of the aryl groups (see atoms from light to dark green in **Figure S9**). On the other hand, the map of electrostatic potential, that allows to visualize variably charged regions within a molecule, shows the distribution of the positive charge especially over the carbon atoms chain linking the two redox centres of the radical cation species (**Figure S10**). The relatively low value of the first oxidation potential of CS03 and CS01 is due to the above electron coupling, being further lowered by the presence of electron donating methoxy groups on the phenyl rings (Table 2). Electron coupling stabilization of the radical cation does not efficiently occur in the other systems (lower K_{CO}) with the longer Ph-BT-Ph bridge, which exhibits higher oxidation potentials and a tiny electrochemical splitting. In the case of LCS01 the unpaired electron is mainly localized only on one donor arylamine redox centre, but the charge is mainly stabilized by the electron donating effect of the methoxyphenyl groups (Figure S9 and S10). In the EP02, thought the positive charge seems to be more delocalized across the molecule, the absence of the electron donating methoxy groups further contributes to enhancing its oxidation potential to a value close to that typical of monoarylamines (Table 2).[21,53,55]

2.3. Electrochromism

Measurements of the absorption and emission spectra under an electrochemical bias (spectroelectrochemistry), were performed in a quartz cuvette of 1 mm optical path, containing a dichloromethane solution of each compound (0.5-1 mM) and $TBAPF_6$ (0.1 M) as supporting electrolyte. The electrochemical bias was controlled by a three-electrode setup, formed by a platinum (Pt) mesh working electrode, a Pt wire counter electrode, and an Ag/Ag^+ pseudo reference electrode, inserted into the cuvette. The UV-Vis spectra of all compounds at 0 V (**Figure 3**) show the distinctive absorption bands already described (Figure 2). Under these conditions, the BTDPA systems exhibit a light pink coloration, while the BTTPA ones display an orange hue (**Figure 4**), according to the optical energy gaps, E_g^{opt}, estimated from the onsets of the lowest energy absorption band (Table 2). In the NIR region, no absorption bands were detected at 0 V. Upon oxidation, all compounds give rise to profound changes in the Vis and NIR regions (Figure 3), accompanied by significant colour switches from light pink to cobalt blue, and from orange to dark green (Figure 4). The electrochromic response of the BTDPAs is very similar, showing the growth of a broad Vis-NIR structured absorption from about 700 nm up to 2000 nm, upon the formation of the radical cation species (0.5 – 0.8 V). With further potential increase, the NIR band is gradually bleached, with the generation of the dication species, and we observe the simultaneous growth of a band at 400-500 nm and a broad absorption in the Vis-NIR range from about 600 nm up to 1000 nm for the CS03 and to 2000 nm for the CS01. The first NIR band, associated to the radical cation species, is the typical optically induced intervalence charge transfer transition (IVCT), and can be clearly distinguished in the spectroelectrochemistry of CS03 (the isosbestic point is at 910 nm). Indeed, the simulated absorption spectra of the radical cation species evidence the IVCT formation for CS03 at about 1100 nm (**Table S8**). In the CS01, the IVCT is less intense and is hidden by the huge absorption of the dication species (ε = 7500 M^{-1} cm^{-1}), covering almost the whole NIR range up to 2000 nm (Figure 3b). A very weak IVCT is still detectable for LCS01 (Figure 3d; isosbestic point at about 1700 nm), while, for the EP02 it can be hardly identified from the NIR absorption of the dication species, which grows almost simultaneously, starting from voltages close to the first oxidation potential. TDDFT calculations, indeed, show that the NIR transitions of the BTTPA monocation species have a strong N-to-bridge-charge transfer (NBCT) character. Therefore, in contrast to most of the D – π – D mixed valence systems already reported, here we highlight that, even when the IVCT band can be clearly distinguished as in the case of CS03 and LCS01, it is always partially overlapped with the absorption of the dication species (**Figure S11** and **Table S8**). This suggests that the benzothiadiazole bridge

may acts as an electron transfer mediator between the arylamine redox centers, due to its electron deficient nature, favouring NBCT processes which occur along with the IVCT (Table S8).

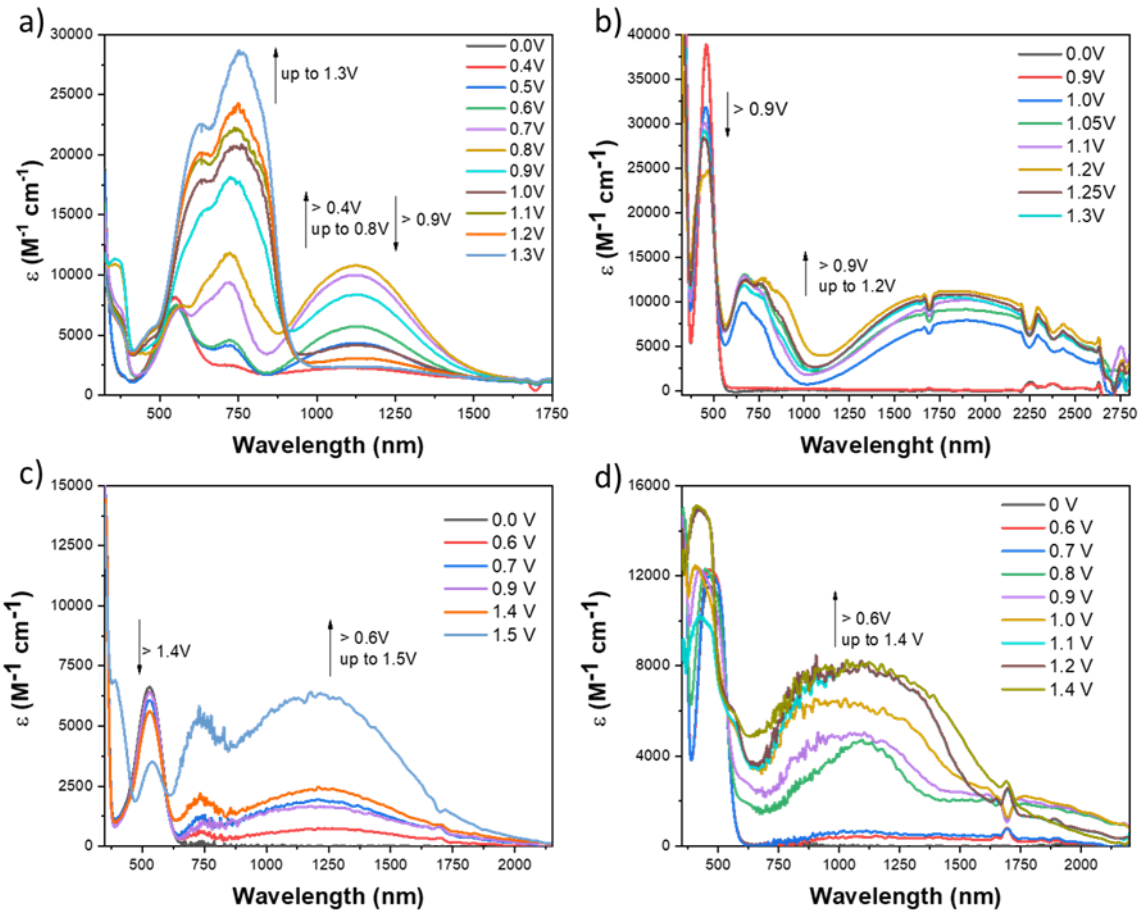

Figure 3. Spectroelectrochemistry of a) CS03, b) CS01, c) EP02, and d) LCS01 in dichloromethane solutions (0.5-1 mM) and TBAPF6 (0.1 M). The potentials are referenced to the AgCl/Ag electrode. Up and down facing arrows indicate, respectively, the growth and the bleaching of the band.

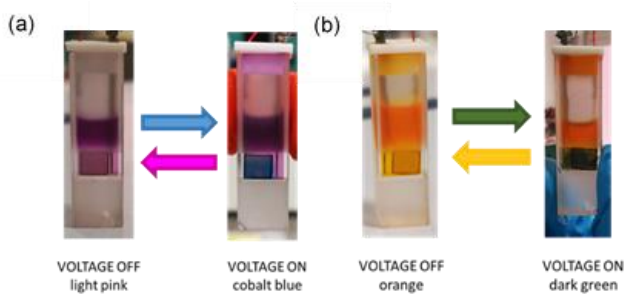

Figure 4. Photographs that display the reversible colour changes of (a) CS03 and CS01 and (b) EP02 and LCS01.

In the case of CS01 and EP02, the spectra of the two ionic species (mono and dication) are practically indistinguishable in the red-NIR range (Figure S10). This situation resembles that observed in dibenzofulvene MVs where the experimental spectrum of the dication species could be described only by the coexistence of singlet and triplet electronic configuration in the ground state.[64] This may also explain the broad absorption in the NIR up to 3000 nm. Indeed, the singlet and triplet states of both EP02 and CS01 are actually separated by a small energy difference, with the triplet more stable than the singlet in EP02 (Table S7).

2.4. Electrofluorochromism

Electrofluorochromism was demonstrated in dichloromethane solution for CS01, LCS01 and EP02, which have a relatively high photoluminescence quantum yield (Table 1). The application of oxidative potentials causes a marked quenching of the whole emission band, which is fully recovered after switching off the potential (**Figure 5**). **Figure 6** displays the % change in the fluorescence (ΔFL %; eq. 1)[23] as a function of the potential applied. The % quenching undergoes a stepwise increase with the formation of the radical cation species, for CS01 and LCS01, and is almost complete (100%) when it is fully generated. In the case of the EP02, the onset for quenching is observed only at potentials where the radical cation and the dication species are both already formed and complete quenching occurs at higher potentials.

$$\Delta FL\% = \left(\frac{A_{off} - A_{on}}{A_{off}}\right) \times 100 \qquad (1)$$

$$CR\ (\Delta\lambda) = \frac{A_{off}}{A_{on}} \qquad (2)$$

where A_{off} and A_{on} are the areas of the fluorescence band in the off and on state, respectively.
A record high electrofluorochromic contrast ratio (eq. 2)[23] of 1230 was obtained with the EP02 system and moderate to very high contrasts with the other mixed valence systems ($64 \leq CR \leq 530$), at potentials from 0.8 to 1.2 V *vs.* AgCl/Ag. Thus, the electrofluorochromic mechanism is very efficient in these BTTPA systems. Moreover, even if the FL quenching involved the whole emission band, a closer inspection of the electrofluorochemistry in Figure 5, suggests that the quenching is more efficient in the red-NIR range. In order to quantitatively evaluate this non-uniform fluorescence quenching, we measured the shift in the emission upon electrochemical oxidation, by calculating the CIE coordinates (CIE 1936) as a function of the potential. **Figure S12** shows, indeed, that the light emitted from the cell, systematically shifts toward green at increasing voltages. This multicolour

electrofluorochromic effect is different from the one that can be obtained by using two different electrofluorochromic materials combined in the same device, as that achieved with thin electrofluorochromic (EF) films of polyfluorene (PFO) and poly(propylenedioxythiophene–phenylene) (P(ProDOT-Ph)),[65] or the "turn on" EFC effect based on pH sensitive luminescent materials, such as the RGB color-tunable EFC devices developed by using the p-benzoquinone as the electro-base redox active molecule, which is able to switch the pH sensitive fluorophores 7-hydroxycoumarin, rhodol, and (2-(2-(4-hydroxystyryl)-6-methyl-4H-pyran-4-ylidene)malononitrile, with blue, green and red fluorescence respectively.[66]

Even though, a shift of the emission band due to electrofluorochromism has already been reported, it has never been investigated in details.[23] In most of the cases, indeed, only slight shifts (~ 20 nm) were reported or can be estimated, and no mechanism were inferred (**Table S9** and references therein). Here we observed a reversible tuning of the fluorescent light over a relatively large spectra range, which is worth to be highlighted and further investigated for the potential exploitation in several technologies.

The decrease in fluorescence along with the blue shift in emission begins with the depletion of the neutral species by its electrochemical oxidation to the radical cation one, which has the electronic configuration schematized in Figure 6b. In the neutral state, the formation of the electronic excited state occurs by absorption of a photon with wavelength < 550 nm. Non-radiative deactivation to the charge transfer state (dotted arrow), with the subsequent radiative deactivation to the ground state, leads to emission in the red-NIR range (red arrow). In contrast, upon excitation of the radical cation (and dication) species from the singly occupied molecular orbital (SOMO) or from the low energy filled molecular orbital (HOMO-1) to the LUMO, fluorescence from the LUMO to either the SOMO or HOMO-1 would energetically correspond to the observed blue shifted emission. Fluorescence from the charge transfer state to the SOMO may also occur in the radical cation species. Indeed, the CT state is still active in the radical cation species even though it is slightly bleached and blue shifted in LCS01 and EP02, and slightly bleached in CS01, with respect to those of the corresponding neutral species (Figure 6 and Figure S10). However, promotion of an electron from the HOMO-1 to the (SOMO) (the IVCT transition),[67-68] may affect the efficiency of the above radiative deactivation processes, explaining the fluorescence quenching observed. Interestingly, in CS01 and LCS01, the generation of the dication species causes an almost total bleaching of the CT absorption (see also the TDDFT data reported in Table S8), thus hampering the fluorescence from the CT state. As a consequence, a significant blue shift of the fluorescence occurs in the above systems on further oxidation to the dication species, where the emission from the localized excited state is predominant.

It is worth to underline that this shift is underestimated because the NIR portion of the fluorescence, does not enter in the calculation of the CIE coordinates.

A direct evidence of the quenching/green shift emission is provided by the acquisition of the fluorescence spectra of the radical cation species produced, *in situ*, by chemical oxidation. **Figure S13** shows the progressive quenching of the fluorescence by stepwise addition of $SbCl_5$ in the reaction cuvette. At the equivalent point (indicated by an arrow), only the radical cation is present in the cuvette and its corresponding spectrum is blue-shifted relatively to that of the neutral species (Figure S13a). Upon further addition of the oxidizing agent, the shift increases, mostly for LCS01 and CS01, according to what observed by electrochemical oxidation (EFC effect). The shift toward the green region is further demonstrated by the CIE diagrams (CIE 1936) (Figure S13b), which highlight how it is more marked for LCS01 and CS01 molecules.

The mechanism of this interesting electroluminochromic effect, which can be potentially exploited in diverse applications, could be inferred by considering that the introduction of the positive charge upon oxidation of the arylamine, hampers the TICT process, leading to a destabilization of the excited conformers with the highest polarity and with the most red-shifted emission.

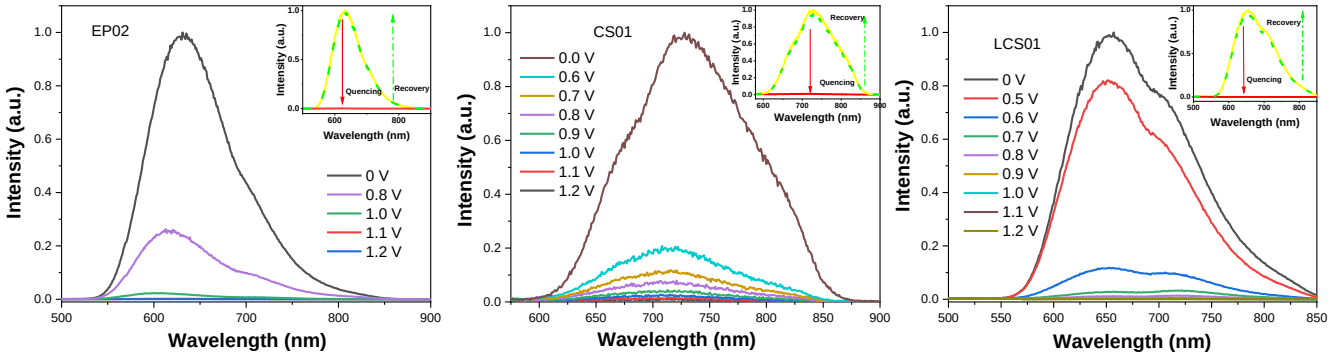

Figure 5. Fluorescence spectra of EP02 (λ_{ex} = 460 nm), CS01 (λ_{ex} = 532 nm) and LCS01 (λ_{ex} = 467 nm) in dichloromethane (0.5-1 mM) and $TBAPF_6$ (0.1 M) as a function of the applied voltages.

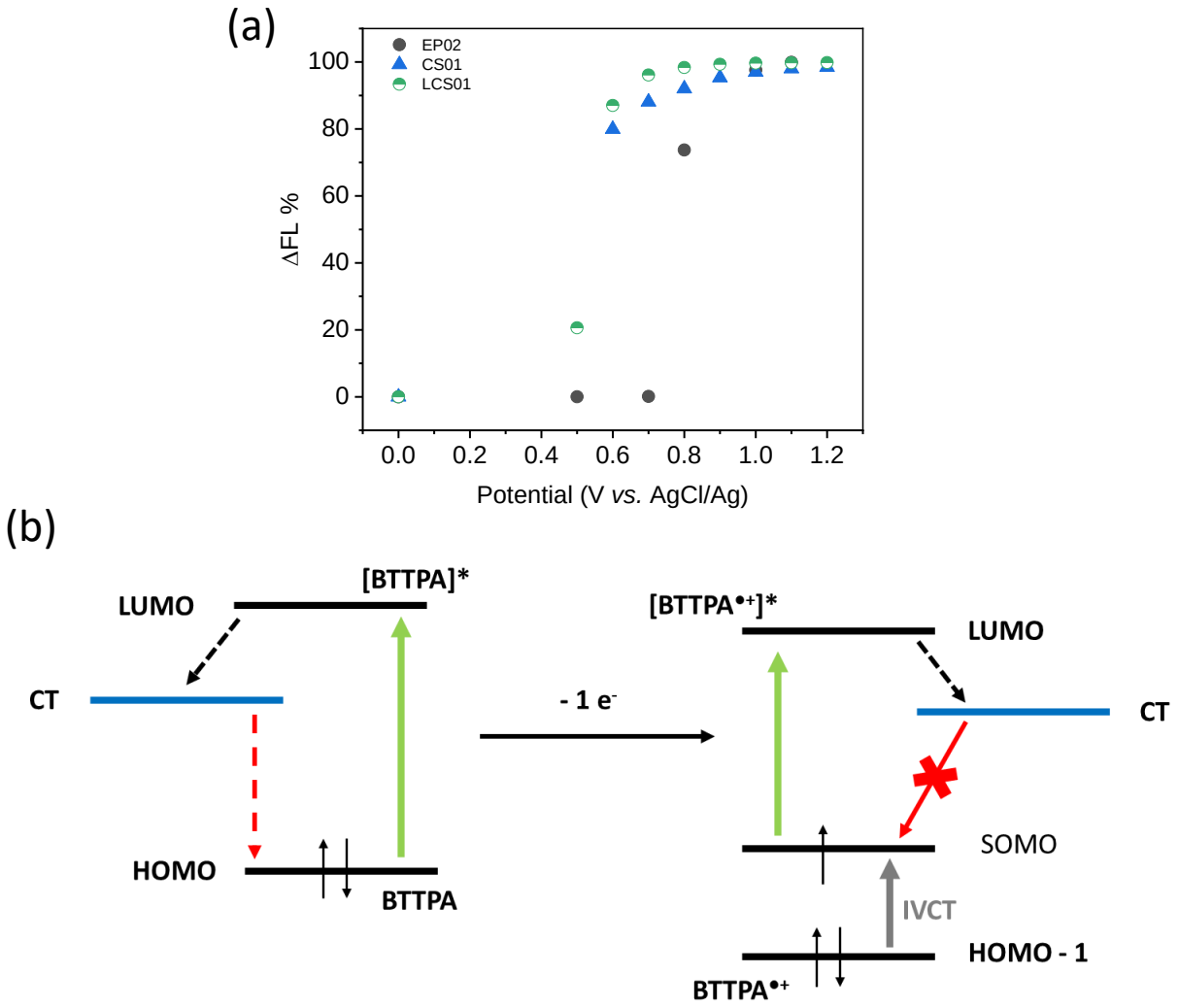

Figure 6. (a) Percentage change in the fluorescence as a function of the potential for EP02, CS01 and LCS01. (b) Schematic hypothesis of the electrofluorochromic quenching mechanism in the BTTPA systems

3. Conclusion

In summary, here we showed the possibility to combine the properties of arylamine MVs with that of photoinduced twisted intramolecular charge transfer fluorophores, in a series of donor-acceptor-donor triads where, the donor units are arylamine derivatives and the acceptor one is an electron-deficient benzothiadiazole bridge. In this way, we obtained compounds with low oxidation potentials, radical cation mixed valence states that are stabilized by relatively strong electron coupling, good fluorescence quantum yields especially in nonpolar solvents and a voltage dependent electroluminochromic quenching mechanism producing a colour tuning of the fluorescence emission from NIR to green.

4. Experimental Section

4.1. Materials and Methods.

Compounds: N^4,N^4,N^7,N^7-tetrakis(4-methoxyphenyl)benzo[c][1,2,5]thiadiazole-4,7-diamine: CS03; N^4,N^4,N^7,N^7-tetrakis(2',4'-dimethoxy-[1,1'-biphenyl]-4- yl)benzo[*c*][1,2,5]thiazole-4,7-diamine: CS01, 4,4'-(benzo[1,2,5]thiadiazole-4,7-diyl)bis(N,N-diphenylaniline): EP02, and N,N'-(benzo[c][1,2,5]thiadiazole-4,7-diylbis(4,1-phenylene)) bis(N-(2',4'-dimethoxy-[1,1'-biphenyl]-4-yl)-2',4'-dimethoxy-[1,1'-biphenyl]-4-amine): LCS01 were synthesized freshly before use.[31,32]

4.2. Electrochemistry and spectroelectrochemistry (absorption and emission).

Electrochemical characterization of all compounds was carried out by cyclic voltammetry (CV) using a AMEL s.r.l. (Mod. 7050) potentiostat. A typical three-electrode cell was assembled with a glassy carbon disk-working electrode, a Pt-wire auxiliary electrode, and an Ag/AgCl nonaqueous reference electrode. Cyclic voltammograms were acquired at different scan rate, from 50 to 100 mV s^{-1}, on 1 mM compound solutions prepared in the electrolyte solution, which consisted of 0.1 M tetrabutylammonium hexafluorophosphate ($TBAPF_6$) in dichloromethane (CH_2Cl_2). All the solutions were previously degassed with N_2. The CV of the ferrocenium/ferrocene (Fc^+/Fc) couple (0.1 mM) was also recorded in the same condition used for the MV compounds solutions and used as external reference for potential calibration. Spectroelectrochemical experiments were performed with an electrolytic cell (BAS Inc.) composed of a 1 mm path length cuvette, where a platinum gauze thin layer and a platinum wire were used as the working electrode and the auxiliary electrode, respectively.[60] A pseudoreference electrode consisting of an Ag wire was calibrated against the Fc^+/Fc redox couple. The spectroelectrochemical cell was filled with dichloromethane solutions of each compound (0.2 mM) and TBAPF6 (0.1 M). UV−vis−NIR spectra were recorded using a Vertex 80 (Bruker) spectrophotometer. The potential was supplied by means of an Amel 2049 model potentiostat. Measurements were performed at 25 °C. Spectroelectrochemistry in emission was performed with the same three-electrode set-up. Uncorrected emission spectra were obtained by Spectrofluorimeter Cary Eclipse Varian (EL 03097953).

4.3. Chemical oxidation

Titration with $SbCl_5$ (Sigma Aldrich) was performed by stepwise additions of the oxidant in CH_2Cl_2 solution (1 mM) using a microliter syringe (Hamilton), directly into a 10 X 10 mm quartz-cuvette with Teflon stopper (Hellma), for UV/Vis/NIR spectroscopy monitoring using a Varian-Cary 5000 UV–Vis–NIR absorption spectrometer. Under these conditions, the low concentration of the oxidant ensures that the oxidation of the DAD compounds proceeds via a 1e- transfer pathway, avoiding the

$SbCl_5$ ligand disproportionation occurring at higher concentration (>20 mM), which eventually leads to the formation of the $SbCl_4^+$ complex, a powerful chlorinating reagent for aromatic hydrocarbons.[69]

4.4. Photophysics.

Absorption spectra were recorded by a Cary Uv-Vis 4000 spectrophotometer. For luminescence experiments, the samples were placed in fluorimetric 1-cm path quartz cuvettes. Uncorrected photoluminescence spectra were obtained with an Edinburgh FLS980 spectrometer equipped with a peltier-cooled Hamamatsu R928 photomultiplier tube (185-850 nm). An Edinburgh Xe900 450 W Xenon arc lamp was used as exciting light source. Corrected spectra were obtained *via* a calibration curve supplied with the instrument. Luminescence quantum yields (Φ_{em}) in solution obtained from spectra on a wavelength scale (nm) were measured according to the approach described by Demas and Crosby[70] using air-equilibrated $[Ru(bpy)_3Cl_2$ in water solution $\Phi_{em} = 0.028$ as standard.

Emission lifetimes in the ps-μs range were determined with the single photon counting technique by means of the same Edinburgh FLS980 spectrometer using a laser diode as excitation source (1 MHz, λ_{exc} = 407, 550 or 635 nm) and an Hamamatsu MCP R3809U-50 (time resolution 20 ps) as detector. Or, with an IBH single photon counting spectrometer equipped with a thyratron gated nitrogen lamp working in the range 2–40 kHz (λ_{exc} = 337 nm, 0.5 ns time resolution) or by using pulsed NanoLED excitation sources at 278 nm, 331 nm, 465 nm, and 560 nm (pulse width ≤ 0.3 ns). Analysis of the luminescence decay profiles vs time was accomplished with the DAS6 Decay Analysis Software provided by the manufacturer.

To record the 77 K luminescence spectra, the samples were put in glass tubes (2 mm diameter) and inserted in a special quartz dewar, filled up with liquid nitrogen.

Experimental uncertainties are estimated to be ± 8% for lifetime determinations, ± 20% for emission quantum yields, ± 2 nm and ± 5 nm for absorption and emission peaks, respectively.

4.5. Computational Details.

All the calculations were done by using Gaussian16 package.[71] Density functional theory (DFT) and its time-dependent extension (TDDFT) were selected for the optimization and the simulation of the absorption spectra, respectively. The hybrid functional PBE0,[72] in combination with def2-TZVP basis set,[73,74] was used to obtain the minima structures of neutral, radical cation and dication (both singlet and triplet) species. The impact of the dichloromethane solvent was taken into consideration by SMD model,[75] employing a dielectric constant of 8.93. The long-range corrected cam-B3LYP functional,[76] coupled with the same basis set, was, instead, employed to characterize the absorption

spectra, as it is previously reported that it can provide a better representation of the absorption bands involving charge-transfer.[77] Unrestricted calculations were used for the open-shell systems, such radical cation species and no spin contamination was found, being the $\langle S^2 \rangle$ value about 0.750 in all cases and 2.0 in the case of triplet dication species.

The symmetry axes of the ellipsoid shape of the investigated molecules, used to calculate the dipole moments, were determined with VMD software[78] by embedding each molecule within a box that took into consideration the van der Waals radii of the atoms constituting the molecule.

Supporting Information

Supporting Information is available from the Wiley Online Library or from the author.

Acknowledgements

The authors are grateful to the Ministero dell'Istruzione dell'Università e della Ricerca Italiano (MIUR) and the University of Calabria for supporting this project in the framework of the ex 60% budget grant. Funding from MINECO (project PID2019-109389RB-I00) and SGR-AGAUR (project 2017SGR00978) is also acknowledged. E.P. is also thankful to ICIQ, CERCA, and ICREA for financial support. D.A.G. acknowledges financial support from MINECO predoctoral fellowship (BES-2017-082439).

References

[1] Y. Kim, E. Kim, G. Clavier, P. Audebert, *Chem. Commun.* **2006**, 3612.

[2] Y. Sun, M. Shi, Y. Zhu, I. F. Perepichka, X. Xing, Y. Liu, C, Yan and H. Meng, *ACS Appl. Mater. Interfaces* **2020**, *12*, 24156.

[3] R. J. Mortimer, D. R. Rosseinsky and P. M. S. Monk, *Electrochromic Materials and Devices,* Wiley-VCH: Weinheim, Germany, **2015**.

[4] A. Beneduci, S. Cospito, M. La Deda and G. Chidichimo, *Adv. Funct. Mater.* **2015**, *25*, 1240.

[5] A. M. Österholm, D. E. Shen, J. A. Kerszulis, R. H. Bulloch, M. Kuepfert, A. L. Dyer and J. R. Reynolds, *ACS Appl. Mater. Interfaces* **2015**, *7*, 1413.

[6] W.-H. Wang, J.-C. Chang and T.-Y. Wu, *Org. Electron.* **2019**, *74*, 23.

[7] H.J. Byker, Single-Compartment, Self-Erasing, Solution-Phase Electrochromic Devices, Solutions for Use Therein, and Uses Thereof. Google Patents US4902108A, 20 February **1990**.

[8] D. R. Rosseinsky and R. J. Mortimer, *Adv. Mater.* **2001**, *13*, 783.

[9] C. Schoot, and J. Ponjee, Image Display Apparatus. US 3806229, 23 April **1974**.

[10] C. Schoot, J. Ponjee, H. Van Dam, R. Van Doorn, and P. Bolwijn, *Appl. Phys. Lett.* **1973**, *23*, 64.

[11] Barclay, D.; Bird, C.; Kirkman, D.; Martin, D.; Moth, E. An integrated electrochromic data display. *Sid 80 Dig.* **1980**, *124*, 124.

[12] Kenworthy, J. Variable Light Transmission Device. US3712709A, 23 January **1973**.

[13] T. G. Yun, M. Park, D. H. Kim, D. Kim, J. Y. Cheong, J. G. Bae, S. M. Han and I. D. Kim *ACS Nano* **2019**, *13*, 3141.

[14] K. W. Shah, S.X. Wang, D. X. Y. Soo and Jianwei Xu, *Polymers* **2019**, *11*, 1839.

[15] P. M. Beaujuge and J. R. Reynolds, *Chem. Rev.* **2010**, *110*, 268.

[16] J. Sun, Y. Chen and Z. Liang, *Adv. Funct. Mater.* **2016**, *26*, 2783.

[17] L. Wu, Y. Sun, K. Sugimoto, Z. Luo, Y. Ishigaki, K. Pu, T. Suzuki, H. Y. Chen and D. Ye, *J. Am. Chem. Soc.* **2018**, *140*, 16340.

[18] S. Zhao, W. Huang, Z. Guan, B. Jin, D. Xiao, *Electrochim. Acta* **2019**, *298*, 533.

[19] P. Andersson, R. Forchheimer, P. Tehrani, M. Berggren, *Adv. Funct. Mater.* **2007**, *17*, 3074.

[20] Y. Alesanco, J. Palenzuela, A. Vinuales, G. Cabanero, H. J. Grande, I. Odriozola, *ChemElectroChem* **2015**, *2*, 218.

[21] A. Beneduci, G. A. Corrente, E. Fabiano, V. Maltese, S. Cospito, G. Ciccarella, G. Chidichimo, G. Gigli and Capodilupo, *Chem. Commun.* **2017**, *53*, 8960.

[22] A. Heckmann, C. Lambert, *Angew. Chem. Int. Ed.* **2012**, *51*, 326.

[23] G.A. Corrente and A. Beneduci, *Adv. Opt. Mater.* **2020**, *8*, 2000887.

[24] G.A. Corrente, E. Fabiano, M. La Deda, F. Manni, G, Gigli, G. Chidichimo, A. L. Capodilupo, A. Beneduci, *ACS Appl. Mater Interfaces* **2019**, *11*, 12202.

[25] P. Audebert, F. Miomandre, *Chem. Sci.* **2013**, *4*, 575.

[26] H. Al-Kutubi, H. R. Zafarani, L. Rassaei, K. Mathwig, *Eur. Polym. J.* **2016**, *83*, 478-498.

[27] H.-J. Yen, G.-S. Liou, *Prog. Polym. Sci.* **2019**, *89*, 250.

[28] Chua, M.H.; Zhu, Q.; Shah, K.W.; Xu, J. *Polymers* **2019**, *11*, 98.

[29] G.A. Corrente, F. Parisi, V. Maltese, S. Cospito, D. Imbardelli, M. La Deda, A. Beneduci, *Molecules* **2021**, *26*, 6818.

[30] M. Wałęsa-Chorab, M. H. Tremblay, M. Ettauoussi, W. G. Skene, *Pure Appl. Chem.* 2015, *87*, 649.

[31] C. Rodríguez-Seco, S. Biswas, G. D. Sharma, A. Vidal-Ferran, and E. Palomares, *J. Phys. Chem. C* **2018**, *122*, 13782.

[32] C. Rodríguez-Seco, M. Méndez, C. Roldán-Carmona, L. Cabau, A. M. Asiri, M. K. Nazeeruddin, and E. Palomares, *ACS Appl. Mater. Interfaces* **2020**, *12*, 32712.

[33] D. K. Sagdullina, I. E. Kuznetsov, A. V. Akkuratov, L. I. Kuznetsova, S. I. Troyanov, P. A. Troshin, *Synth. Met.* 2019, *250*, 7.

[34] K. Mahesh, S. Karpagam, T. Putnin, H. Le, T.-T. Bui, K. Ounnunkad, F. Goubard, *J. Photochem. Photobiol. A* 2019, *371*, 238.

[35] F. Wu, Y. Ji, R. Wang, Y. Shan, L. Zhu, *Dyes Pigm.* 2017, *143*, 356.

[36] F. Wu, Y. Ji, C. Zhong, Y. Liu, L. Tan, L. Zhu, *Chem. Commun.* 2017, *53*, 8719.

[37] S. Shen, L. Gao, C. He, Z. Zhang, Q. Sun, Y. Li, *Org. Electron. physics, Mater. Appl.* 2013, 14, 875.

[38] M. Thelakkat, *Macromol. Mater. Eng.* 2002, 287, 442.

[39] D. H. Lee, M. J. Lee, H. M. Song, B. J. Song, K. D. Seo, M. Pastore, C. Anselmi, S. Fantacci, F. De Angelis, M. K. Nazeeruddin, M. Gräetzel, H. K. Kim, *Dyes Pigm.* 2011, *91*, 192.

[40] T. Ghanem, T. Vincendeau, P. S. Marqués, A. H. Habibi, S. Abidi, A. Yassin, S. Dabos-Seignon, J. Roncali, P. Blanchard, C. Cabanetos, *Mater Adv.* 2021, *2*, 7456.

[41] P. F. Xia, J. Lu, C. H. Kwok, H. Fukutani, M. S. Wong, Y. Tao, *J. Polym. Sci. A Polym. Chem.* 2009, *47*, 137.

[42] P. Zheng, J. Xu, F. Peng, S. Peng, J. Liao, H. Zhao, L. Li, X. Zeng, H. Yub *New J. Chem.* 2021, *45*, 4443.

[43] S. Paek, N. Cho, K. Song, M.-J. Jun, J. K. Lee, J Ko. *J. Phys. Chem. C* 2012, *116*, 23205.

[44] Z. Peng, K. Zhang, Z. Wang, S. Duttwyler, Y. Wang, P. Lu, *J. Mater. Chem. C* 2019, *7*, 2430.

[45] A. Pathak, K. R. J. Thoms, M. Singh, J,-H. Jou, *J. Org. Chem.* 2017, *82*, 11512.

[46] K. R. J. Thomas, T.-H. Huang, J. T. Lin, S –C. Pu, Yi-M. Cheng, C.-C. Hsieh, C. P. Tai, *Chem. Eur. J.* 2008, *14*, 11231.

[47] A. Pazini, L. Maqueira, H. C. Avila, F. M. Valente, R. E. Aderne, D. Back, R. Q. Aucélio, M. Cremona, J. Limberger, *Tetrahedron Lett.* 2018, *59*, 2994.

[48] K. R. J. Thomas, M. Velusamy, J. T. Lin, S.-S. Sun, Y.-T. Tao, C.-H. Chuen, *Chem Commun.* 2004, 2328.

[49] A. J. A. B. Seeley, R. H. Friend, J.-S. Kim, *J. Appl. Phys.* 2004, *96*, 7643.

[50] B. A. D. Neto, J. R. Correa, J. Spencer. *Chem. Eur. J.* **2022**, *28*, e202103262.

[51] H. Lim, S. Seo, S. Pascal, Q. Bellier, S. Rigaut, C. Park, H. Shin, O. Maury, C. Andraud, E. Kim, *Sci. Rep.* **2016**, *6*, 18867.

[52] L. N. Ma, H. J. Niu, J. W. Cai, P. Zhao, C. Wang, X. Bai, Y. Lian, W. Wang, *Carbon* **2014**, *67*, 488.

[53] M. Thelakkat, *Macromol. Mater. Eng.* **2002**, *287*, 442.

[54] S. Seo, S. Pascal, C. Park, K. Shin, X. Yang, O. Maury, B. D. Sarwade, C. Andraud, and E. Kim, *Chem. Sci.* **2014**, 5(4), 1538.

[55] S. Kim and Y. You, *Adv. Optical Mater.* **2019**, *7*, 1900201.

[56] A. Iagatti, B. Patrizi, A. Basagni, A. Marcelli, A. Alessi, S. Zanardi, R. Fusco, M. Salvalaggio, L. Bussotti, P. Foggi, *Phys. Chem. Chem. Phys.* **2017**, *19*, 13604.

[57] J. Pina, J. Seixas de Melo, D. Breusov, U. Scherf, Phys. Chem. Chem. Phys. 2013, 15, 15204.

[58] B. Sk, M. Sarkar, K. Singh, A. Sengupta, A. Patra, *Chem. Commun.* **2021**, *57*, 13590.

[59] Y. Wang, K. B. Eisenthal, *J. Chem. Phys.* **1982**, *77*, 6076.

[60] a) G. A. Corrente, E. Fabiano, F. Manni, G. Chidichimo, G. Gigli, A. Beneduci, A.-L. Capodilupo, *Chem. Mater.* **2018**, *30*, 5610; b) V. Maltese, S. Cospito, A. Beneduci, B. C. De Simone, N. Russo, G. Chidichimo, and R. A. J. Janssen, *Chem. - Eur. J.* 2016, **22**, 10179; c) S. Cospito, A. Beneduci, L. Veltri, M. Salamonczyk, and G. Chidichimo, *Phys. Chem. Chem. Phys.*, 2015, **17**, 17670.

[61] B. Patrizi, A. Iagatti, L. Abbondanza, L. Bussotti, S. Zanardi, M. Salvalaggio, R. Fusco, P. Foggi, *J. Phys. Chem. C* 2019, *123*, 5840.

[62] N. Pandey, M. S. Mehata, S. Pant, N. Tewari, *J. Fluoresc.* **2021**, *31*, 1719.

[63] A. Kawski, *Z. Naturforsch.* 2002, 57a, 255.

[64] A. L. Capodilupo, F. Manni, G. A. Corrente, G. Accorsi, E. Fabiano, A. Cardone, R. Giannuzzi, A. Beneduci, G. Gigli, *Dyes Pigm.* **2020**, *177*, 108325.

[65] H. Lim, S. Seo, C. Park, H. Shin, X. Yang, K. Kanazawa, and E. Kim, *Opt. Mater. Express* **2016**, 6, 1808.

[66] X. Wang, W. Li, W. Li, C. Gu, H. Zheng, Y. Wang, Y.-M. Zhang, M. Li and S. X.-A. Zhang, *Chem. Commun.*, **2017**, 53, 11209.

[67] D. T. Breslin, M. A. Fox, *J. Phys. Chem.* **1994**, *98*, 408.

[68] S. Chaudhry, S. M. Ryno, M. Zeller, D. R. McMillin, C. Risko, and J. Mei, *J. Phys. Chem. B* **2019**, 123, 3866.

[69] P. Cársky and R. Zahradnik, *Acc. Chem. Res.* **1976**, *9*, 407.

[70] J. N. Demas, G. A. Crosby, *J. Phys. Chem.* **1971**, *75*, 991.

[71] M. J. Frisch, G. W. Trucks, H. B. Schlegel, G. E. Scuseria, M. A. Robb, J. R. Cheeseman, G. Scalmani, V. Barone, G. A. Petersson, H. Nakatsuji, X. Li, M. Caricato, a. V. Marenich, J. Bloino, B. G. Janesko, R. Gomperts, B. Mennucci, H. P. Hratchian, J. V. Ortiz, A. F. Izmaylov, J. L. Sonnenberg, D. Williams-Young, F. Ding, F. Lipparini, F. Egidi, J. Goings, B. Peng, A. Petrone, T. Henderson, D. Ranasinghe, V. G. Zakrzewski, J. Gao, N. Rega, G. Zheng, W.

Liang, M. Hada, M. Ehara, K. Toyota, R. Fukuda, J. Hasegawa, M. Ishida, T. Nakajima, Y. Honda, O. Kitao, H. Nakai, T. Vreven, K. Throssell, J. A. Montgomery Jr., J. E. Peralta, F. Ogliaro, M. J. Bearpark, J. J. Heyd, E. N. Brothers, K. N. Kudin, V. N. Staroverov, T. A. Keith, R. Kobayashi, J. Normand, K. Raghavachari, A. P. Rendell, J. C. Burant, S. S. Iyengar, J. Tomasi, M. Cossi, J. M. Millam, M. Klene, C. Adamo, R. Cammi, J. W. Ochterski, R. L. Martin, K. Morokuma, O. Farkas, J. B. Foresman, D. J. Fox, 2016, Gaussian 16, Revision C.01, Gaussian, Inc., Wallin.

[72] C. Adamo, V. Barone, *J. Chem. Phys.* **1999**, *110*, 6158.

[73] F. Weigend, *Phys. Chem. Chem. Phys.* **2006**, *8*, 1057.

[74] F. Weigend, R. Ahlrichs, *Phys. Chem. Chem. Phys.* **2005**, *7*, 3297.

[75] A. V Marenich, C. J. Cramer, D. G. Truhlar, *J. Phys. Chem. B* **2009**, *113*, 6378.

[76] T. Yanai, D. P. Tew, N. C. Handy, *Chem. Phys. Lett.* **2004**, *393*, 51.

[77] R. Kobayashi, R. D. Amos, *Chem. Phys. Lett.* **2006**, *420*, 106.

[78] W. Humphrey, A. Dalke, K. Schulten, "VMD - Visual Molecular Dynamics", J. Molec. Graphics, 1996, vol. 14, pp. 33-38.

Molecular triads made by (arylamine)-Donor/(electron deficient fluorophore)-Acceptor/(arylamine)-Donor building blocks are shown here to be a convenient strategy to obtain redox-responsive materials with both vis-NIR electrochromism and red-NIR electroluminochromism with an impressive reversible photoluminescence quenching effect and an efficient voltage-dependent tuning of the color of the light emission

G. A. Corrente, D. A. González, E. Aktas, A. L. Capodilupo, G. Mazzone, F. Ruighi, G. Accorsi, D. Imbardelli, C. Rodriguez-Seco, E. Martinez-Ferrero, E. Palomares, and A. Beneduci*

Vis-NIR electrochromism and NIR-green electroluminochromism in dual functional benzothiadiazole-arylamine mixed-valence compounds